Article

Current Biology

Recruitment of grid-like responses in human entorhinal and piriform cortices by odor landmark-based navigation

Highlights

- Olfactory landmarks can inform human spatial navigation in a virtual environment
- Odor navigation elicits grid-like responses in entorhinal and piriform cortices
- Grid-like responses in entorhinal and piriform cortices share the same grid angle
- Findings suggest the existence of a specialized olfactory grid network

Authors

Clara U. Raithel, Alexander J. Miller, Russell A. Epstein, Thorsten Kahnt, Jay A. Gottfried

Correspondence

raithelc@sas.upenn.edu (C.U.R.), jaygottf@pennmedicine.upenn.edu (J.A.G.)

In brief

Olfactory navigation is universal across the animal kingdom. Raithel et al. show that humans can use odor landmarks to navigate a virtual space, and this behavior is accompanied by grid-like responses in entorhinal and piriform cortices attuned to the same grid angle. These findings suggest the presence of a specialized olfactory grid network.

Raithel et al., 2023, Current Biology *33*, 1–10
September 11, 2023
https://doi.org/10.1016/j.cub.2023.06.087

CellPress

Please cite this article in press as: Raithel et al., Recruitment of grid-like responses in human entorhinal and piriform cortices by odor landmark-based navigation, Current Biology (2023), https://doi.org/10.1016/j.cub.2023.06.087

Current Biology

CellPress
OPEN ACCESS

Article

Recruitment of grid-like responses in human entorhinal and piriform cortices by odor landmark-based navigation

Clara U. Raithel,[1,2,4,*] Alexander J. Miller,[2] Russell A. Epstein,[1] Thorsten Kahnt,[3] and Jay A. Gottfried[1,2,*]
[1]Department of Psychology, University of Pennsylvania, 3450 Hamilton Walk, Philadelphia, PA 19104, USA
[2]Department of Neurology, University of Pennsylvania, 3450 Hamilton Walk, Philadelphia, PA 19104, USA
[3]National Institute on Drug Abuse, Intramural Research Program, 251 Bayview Blvd, Baltimore, MD 21224, USA
[4]Lead contact
*Correspondence: raithelc@sas.upenn.edu (C.U.R.), jaygottf@pennmedicine.upenn.edu (J.A.G.)
https://doi.org/10.1016/j.cub.2023.06.087

SUMMARY

Olfactory navigation is universal across the animal kingdom. Humans, however, have rarely been considered in this context. Here, we combined olfactometry techniques, virtual reality (VR) software, and neuroimaging methods to investigate whether humans can navigate an olfactory landscape by learning the spatial relationships among discrete odor cues and integrating this knowledge into a spatial map. Our data show that over time, participants improved their performance on the odor navigation task by taking more direct paths toward targets and completing more trials within a given time period. This suggests that humans can successfully navigate a complex odorous environment, reinforcing the notion of human olfactory navigation. fMRI data collected during the olfactory navigation task revealed the emergence of grid-like responses in entorhinal and piriform cortices that were attuned to the same grid orientation. This result implies the existence of a specialized olfactory grid network tasked with guiding spatial navigation based on odor landmarks.

INTRODUCTION

Olfactory navigation is paramount across the animal kingdom.[1–3] Despite increasing scientific interest in how animals use olfaction to find their way,[4–13] humans have rarely been considered in this context.[3] It is commonly accepted that humans overwhelmingly use visual cues to navigate their environment, and research on human subjects predominantly focuses on spatial navigation under visual guidance. Contrary to this notion, recent work in human subjects suggests a potential link between spatial memory and olfactory function: in a set of studies,[14,15] spatial navigation performance across subjects was positively correlated with the success of olfactory identification. Interestingly, performance on both tasks could be predicted using cortical thickness measures in the medial orbitofrontal cortex,[14,15] an area receiving direct projections from primary olfactory cortex.[16] These findings support the idea of an intrinsic association between spatial and olfactory abilities,[17] which may result from shared neural substrates.[14]

A handful of experiments investigating human olfactory navigation suggest that humans can in fact use olfactory cues for spatial orientation and navigation. For example, human participants are able to follow scent tracks,[18] exploit differences in odor concentration and/or timing across the two nostrils to optimize behavior,[19–21] represent olfactory objects to inform spatial decisions,[22] and utilize subtle differences in olfactory intensity gradients to encode odor-based cognitive maps.[23,24] These studies highlight the fact that the human olfactory system is not only an odor detection system but can also exploit olfactory cues in the service of odor-based map-building and behavior.

Despite initial evidence showing that olfactory cues can inform spatially guided behaviors in humans, it remains unclear if and how humans use discrete olfactory cues (i.e., olfactory landmarks) to form cognitive maps of their spatial environment. Most importantly, it is unclear whether the principles of map-making in the visual domain[25] are paralleled in the olfactory modality. For example, for cognitive maps to be useful, landmarks are needed to anchor spatial coordinates to fixed aspects of the environment.[25] In principle, such landmarks could be represented by any sensory modality, as long as they are (1) spatially stable and (2) perceptually salient. The idea that olfactory cues may serve as landmarks supporting navigation has been proposed by recent work in rodents,[26] highlighting potential mechanisms by which the mammalian brain accomplishes the integration of olfactory landmarks into cognitive maps. This work identified the tight interplay between olfactory (sensory) cues and path integration as key to the formation of reliable spatial representations in hippocampal place cells. Likewise, entorhinal cortex (ERC) shares close anatomical connections with both the piriform cortex[27–30] and the hippocampus,[30,31] underscoring the potential importance of olfactory landmarks in generating cognitive maps to optimize path finding.

Here, we used olfactometry and virtual reality (VR) tools to investigate whether humans can use olfactory landmarks to generate an internalized map of the environment and whether this map is reliably represented at the neural level. To this end,

Please cite this article in press as: Raithel et al., Recruitment of grid-like responses in human entorhinal and piriform cortices by odor landmark-based navigation, Current Biology (2023), https://doi.org/10.1016/j.cub.2023.06.087

we created an environment in which participants encountered eight discrete odors at eight distinct locations within the VR arena. Participants were tasked with learning the spatial relationships among these odor cues and using this knowledge to navigate more efficiently within the virtual arena. Critically, this experimental design enabled us to test two key hypotheses. At the behavioral level, we predicted that participants would improve their task performance over the course of the experiment, demonstrating their ability to integrate odor landmarks into a coherent map. At the neural level, our prediction was based on the idea that navigation from one location to another would be mediated by grid cells,[32–34] whose activity can serve as a neural marker for cognitive maps. Although we are unable to measure individual cells using functional magnetic resonance imaging (fMRI) techniques, their presence can be inferred using fluctuations in the fMRI blood-oxygenation-level-dependent (BOLD) signal,[35] allowing us to directly address this research question. More specifically, and building on prior findings in both humans[23] and rodents,[11] we predicted that grid-like activity in ERC would mediate odor-guided spatial navigation by recruiting ventromedial prefrontal cortex (vmPFC) and piriform cortex into a specialized olfactory grid network within which information about the identity and location of olfactory landmarks provides the necessary anchoring of the cognitive map.

RESULTS

Humans can navigate virtual space using olfactory landmarks

To test whether humans can use olfactory landmarks to orient and navigate in space, we created a visually ambiguous virtual landscape in which participants were forced to use their sense of smell to locate odorous objects anchored at specific positions in the environment. To this end, we placed eight odors at eight distinct locations in a circular arena. These locations were marked by white clouds hovering over the grassy field of the arena (Figure 1A). Participants were asked to navigate from their current position, i.e., one of the odor clouds, to a specified "target odor" cloud. Once they found the target odor, they were given feedback as well as instructions about which odor to search for next (Figure 1B). Because the spatial odor layout was held constant across trials, blocks, and days, participants were able to learn the spatial relationships among the odors and use this information to find the target odors more quickly over time. Importantly, visual features in the virtual environment, including the perimeter wall marking the boundaries of the arena and the white clouds showing the positions of the eight odors in the arena, were landmark-deficient, such that they could not be used to localize or orient within the space. In other words, the only way to acquire a sense of orientation was to inhale and smell the odors upon entering an odor cloud.

Twenty-eight participants underwent 2 days of behavioral training (days 1 and 2) and subsequently participated in two fMRI scanning sessions (days 3 and 4; Figure 1C). To determine whether participants were able to learn about the spatial layout of olfactory landmarks and improve their performance over time, we assessed path tortuosity, a measure of path indirectness (defined as the distance traveled divided by the Euclidean distance between the start and the target odor cloud; see Figure 2A), across the 4 days of testing. As predicted, participants showed a decrease in path tortuosity (repeated measures ANOVA; $F_{3,\ 81} = 29.33$, $p < 0.001$; Figures 1D and 2A), indicating that participants took more direct paths to the target over the time course of the experiment.

By taking more direct routes to the target, participants were able to complete a greater number of trials across days (repeated measures ANOVA; $F_{3,\ 81} = 84.13$, $p < 0.001$; Figure 2B). Specifically, participants completed more trials per minute both between (effect of day: $F_{3,\ 81} = 84.13$, $p < 0.001$; Figure 2C) and within (effect of minute: $F_{31,\ 837} = 29.138$, $p < 0.001$; Figure 2C) individual sessions. Of note, within-session improvement in task performance "flattened out" across the 4 days of testing (effect of day × minute: $F_{93,\ 2,511} = 2.68$, $p < 0.001$; Figure 2C), indicative of a ceiling effect. Despite this ceiling effect, participants' performance was consistently lower in the first minute of each block compared with all later minutes ($t_{27} > 18.5$, $p < 0.001$), regardless of the day or block (Figure 2C).

Task performance was not influenced by the intensity, pleasantness, or familiarity of the odors (Figures S2A and S2B), such that participants did not perform better navigating toward an odor that was particularly intense, familiar, or pleasant to them. Likewise, task performance did not vary as a function of inhalation duration (Figures S2C and S2D), indicating that participants navigated the environment equally well, irrespective of whether they took a long or short breath. This scenario was expected as the odors were chosen to be easy to identify and of moderate to strong intensity, allowing for effortless odor identification even when inhaling only for a short period of time. Finally, task performance was not influenced by gender (Figures S2E and S2F), although our study was not designed to test for such group comparisons, indicating that female and male participants were performing the task equally well. Note that five participants dropped out of the study after the 2 days of behavioral training due to their inability to reach the performance criteria. Among these five subjects, sub-par performance was found in two males and three females.

Taken together, our behavioral data illustrate that participants were able to learn the spatial relationship between olfactory landmarks and use this knowledge to take more direct paths when navigating toward a specific target. More efficient path-taking is a hallmark of cognitive map-based spatial navigation, indicating that participants developed a mental map of the olfactory virtual environment.

Grid-like responses in ERC during human olfactory navigation

The neural substrates of cognitive maps, including place and grid codes, have been extensively studied in the literature,[25] with the caveat of focusing predominantly on visual landmarks to guide spatial navigation and map formation. Here, we tested whether the human brain uses a grid-like coding scheme to enable navigation from one olfactory landmark to another. Initially, we focused our search on the ERC, an area traditionally associated with grid cell activity in both animals[33] and humans[36] during visually guided navigation. Because entorhinal grid cells share a common grid orientation across neighboring cells[34,35,37,38] and show preferential firing for movements aligned (vs. misaligned) with the main axes of the grid,[35] the presence of grid-like signals in ERC can

Please cite this article in press as: Raithel et al., Recruitment of grid-like responses in human entorhinal and piriform cortices by odor landmark-based navigation, Current Biology (2023), https://doi.org/10.1016/j.cub.2023.06.087

CellPress
OPEN ACCESS

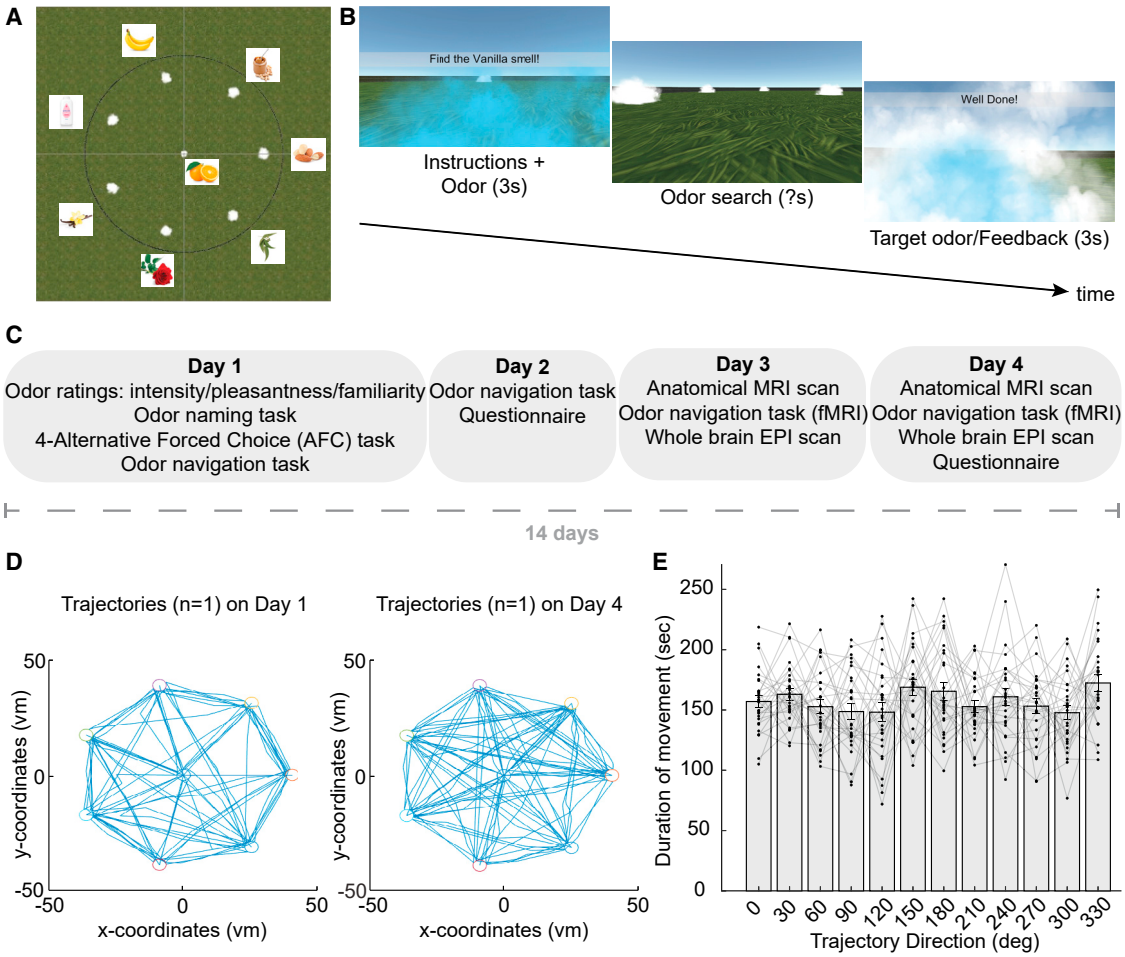

Figure 1. Experimental design

(A) Bird's eye view of the environment. The circular arena was populated with eight distinct odor clouds (orange, almond, peanut butter, banana, baby powder, vanilla, rose, and eucalyptus), one of which was placed in the center; the remaining seven were distributed in the periphery at a distance of 40 virtual meters (vm) from the center. The radius of the arena was set to 50 vm.

(B) Example trial. At the beginning of each block, participants received an instruction informing them which odor they needed to find (i.e., the target odor). At the same time that the instruction appeared, the white cloud changed its color to blue, cueing the participants to smell the odor associated with their current location. After 3 s, both the odor and the instruction screen disappeared, following which the cloud turned white again, and participants were free to move around to search for the target odor. As soon as participants found the target odor, they received feedback ("Well Done!") and a new instruction indicating which odor they needed to seek out next.

(C) Experimental timeline. On day 1, participants completed odor ratings, an odor naming task, a 4-alternative forced choice (AFC) task, and the odor navigation task. On day 2, participants completed the odor navigation task, followed by a short questionnaire to check if they had had sufficient time to smell the odors. Participants whose performance exceeded 50% of the mean performance across all participants were invited for two additional sessions (days 3 and 4) comprised an anatomical MRI scan, an fMRI scanning session during which participants performed the odor navigation task, a whole brain echo-planar image (EPI) scan, as well as a short post-study questionnaire on day 4 only. Participants completed all experimental procedures within a 14-day time span.

(D) Example trajectories from one subject on days 1 (left) and 4 (right). On day 1, the participant was "new" to the task and mostly walked around in a circle in search of the target odor. On day 4, trajectories covered the full range of possible paths, suggesting that the participant took more direct paths to the target odor.

(E) Duration of movement (s) on days 3 and 4 as a function of trajectory direction, divided into twelve 30° bins. Duration of movement (s) was equally distributed across the bins; note however that the corresponding statistical test revealed a trend toward significance (repeated measures ANOVA, $F_{11, 297} = 1.87$, $p = 0.082$). Data are mean ± standard error of the mean (SEM). Dots represent data from individual participants. For further details regarding the (un-)equal sampling of movement trajectories, see also Figure S1.

be inferred from fMRI-based measurements.[35] Our central prediction was that when participants navigated in parallel with their respective ERC grid orientation φ (including trajectories offset by 60° intervals relative to φ), a higher average signal in ERC would be observed in this brain area compared with misaligned trajectories (Figure 3; also see STAR Methods).

To test this hypothesis, we performed a leave-one-out cross-validation analysis, a method commonly used to test for grid-like responses in *a priori*-defined regions of interest (ROIs).[23,39] In this analysis, for every participant, the grid orientation in ERC was estimated using the training dataset consisting of all runs but one (see STAR Methods). In a subsequent step, trajectories

Please cite this article in press as: Raithel et al., Recruitment of grid-like responses in human entorhinal and piriform cortices by odor landmark-based navigation, Current Biology (2023), https://doi.org/10.1016/j.cub.2023.06.087

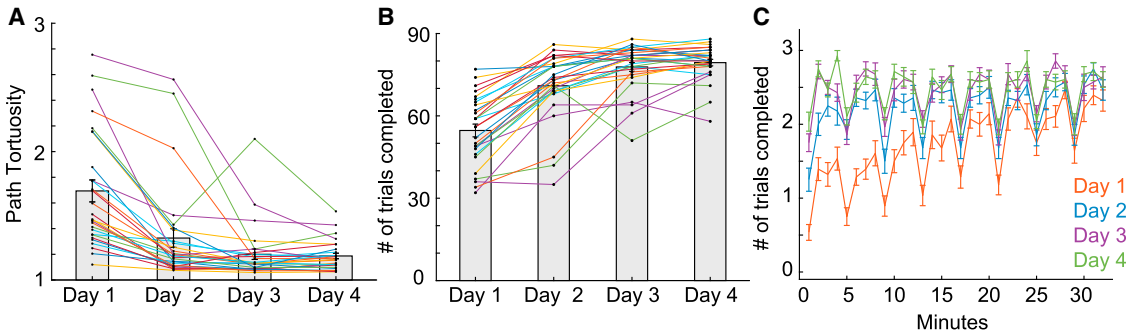

Figure 2. Human spatial navigation based on olfactory landmarks

(A) Path tortuosity across the 4 days of testing. Path tortuosity is a measure of path indirectness and defined as the distance traveled divided by the Euclidean distance between the start and the target odor cloud. A value of 1 reflected perfect performance, whereas increasingly larger values reflected increasingly indirect paths and hence, worse performance. Participants took more direct paths toward the target across days ($F_{3, 81} = 29.33$, $p < 0.001$).

(B) Number of trials completed across the 4 days. Participants gradually improved their performance over time. Repeated measures ANOVA with within-subjects factor "day" yielded a significant effect of day ($F_{3, 81} = 84.13$, $p < 0.001$).

(C) Number of trials completed per minute of the odor navigation task. Participants improved their performance over the time course of a given session (8 blocks × 4 min, resulting in 32 min per session; $F_{31, 837} = 29.138$, $p < 0.001$) and across days ($F_{3, 81} = 84.13$, $p < 0.001$). Participants showed a drop in performance every 4th min, i.e., at the beginning of each block. This effect was first seen on day 1 and persisted through day 4 ($t_{27} > 18.50$, $p < 0.001$). See also Figure S2.

Data are mean ± SEM. Dots represent data from individual participants.

in the test dataset consisting of the left-out run were aligned to the grid orientation obtained from the training dataset and then divided into twelve 30° bins around the unit circle (Figures 3, 4A, and 4B; see STAR Methods). The main hypothesis was that movement along trajectories aligned with the participant's grid orientation (orange trajectories in Figures 3, 4A, and 4B) should produce a greater signal in ERC compared with movement along trajectories misaligned with the grid orientation (blue trajectories in Figures 3, 4A, and 4B). ERC was defined anatomically using a mask in the Montreal Neurological Institute (MNI) space made available online (Figure 4C).[40]

This analysis revealed that ERC signal was consistently higher when navigating along trajectories aligned (vs. misaligned) with the grid orientation φ ($t_{27} = 2.49$, $p_{FDR} = 0.019$, one-sided; Figure 4D), an effect that was specific to 60° periodicity ($t_{27} < 0.65$, $p > 0.262$, one-sided; Figure 4E). Follow-up testing revealed that this effect was driven by activation of the right ERC (rERC) ($t_{27} = 3.43$, $p_{FDR} = 0.002$, one-sided), with left ERC not yielding significant results ($t_{27} = 0.64$, $p_{FDR} = 0.264$, one-sided). A paired t test comparing right and left ERC within subjects revealed a nominal but non-significant difference ($t_{27} = 1.93$, $p = 0.064$; Figure 4F). This result profile was in line with earlier fMRI literature reporting lateralized results for grid-like responses[35,41] during visually cued spatial navigation. Given these findings, we restricted our subsequent analyses to the rERC.

Grid-like responses in APC during human olfactory navigation

Recent fMRI findings indicate that human grid-like activity is not confined to ERC. One robust example is the presence of grid-like fMRI signatures in vmPFC, encompassing physical, perceptual, social, and abstract spaces.[23,35,39,42] Such observations raise the intriguing idea that navigation-based behaviors may engage an entire network of brain regions displaying grid-like activity.

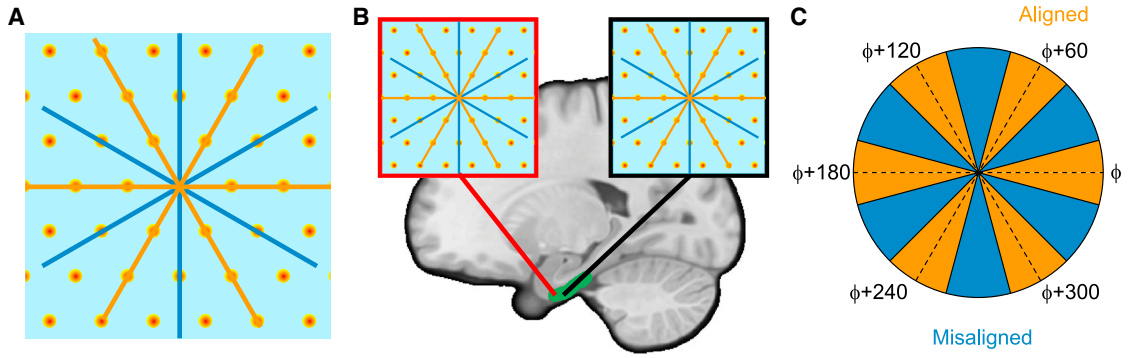

Figure 3. Measuring grid-like responses in the human brain

(A) Firing fields of a single grid cell. One can define three axes that are aligned with the grid (orange) and three axes that are misaligned with the grid (blue). A relatively higher number of firing fields is encountered when navigating along the aligned axes, resulting in higher activity.

(B) Neighboring grid cells in ERC tend to share the same grid orientation.

(C) Hence, one would predict that fMRI BOLD signal should be higher when moving along the aligned (orange) vs. the misaligned (blue) axes.

Please cite this article in press as: Raithel et al., Recruitment of grid-like responses in human entorhinal and piriform cortices by odor landmark-based navigation, Current Biology (2023), https://doi.org/10.1016/j.cub.2023.06.087

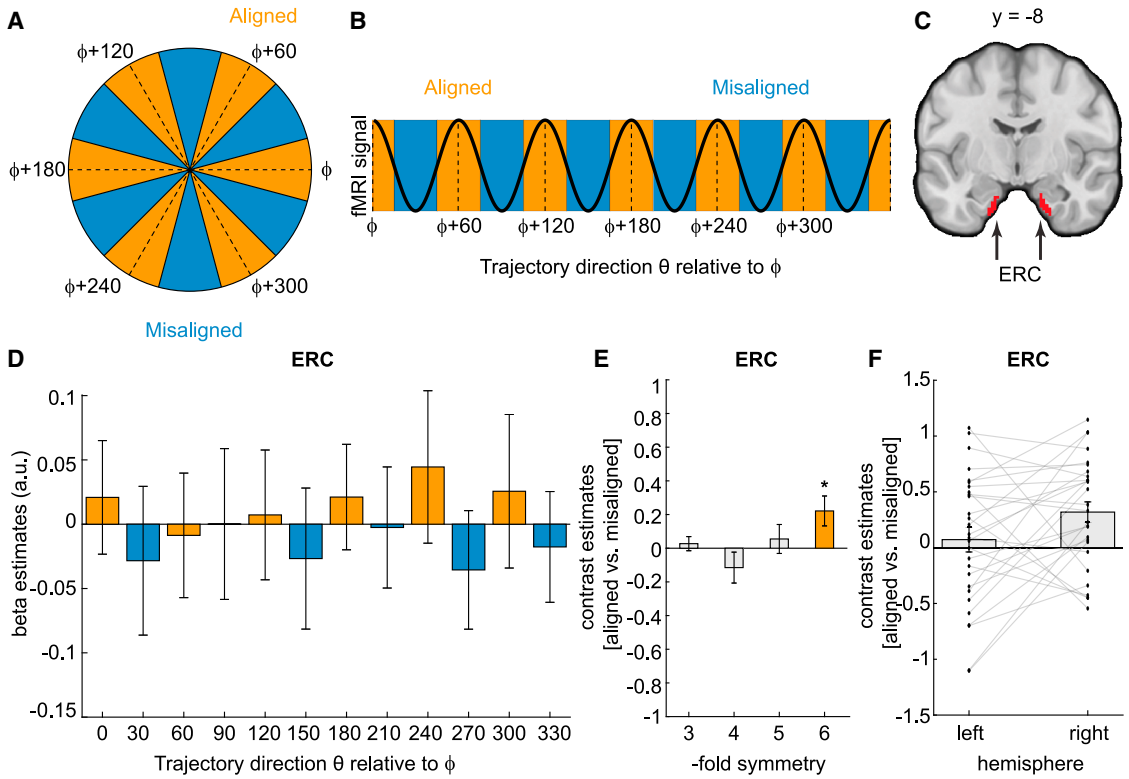

Figure 4. Grid-like responses in entorhinal cortex (ERC) during human olfactory navigation

(A) Analysis schematic. Given a brain area containing grid cells aligned to the grid orientation φ, movement trajectories of a participant can be aligned or misaligned with φ.

(B) Grid-like fMRI BOLD signal is expected to be higher for aligned vs. misaligned trials.

(C) Anatomical mask delineating ERC.[40]

(D) Hexagonally modulated activity was detected in ERC (aligned > misaligned; $t_{27} = 2.49$, $p_{FDR} = 0.019$, one-sided).

(E) Sinusoidal modulation of the fMRI signal in ERC was specific to 6-fold symmetry, i.e., 60° periodicity ($t_{27} < 0.65$, $p > 0.262$, one-sided).

(F) A paired t test comparing right and left ERC within subjects revealed a trend toward significance ($t_{27} = 1.93$, $p = 0.064$). See also Figures S3 and S4.

Data are mean ± SEM. Dots represent data from individual participants.

Our own recent work has further suggested that a primary olfactory region, particularly, the piriform cortex, may be intrinsically involved in helping to establish a cognitive map of olfactory space.[23]

To test whether areas in vmPFC, anterior piriform cortex (APC), or posterior piriform cortex (PPC) manifest grid-like responses during human olfactory navigation, we conducted a leave-one-out cross-validation analysis in these three ROIs, each of which was defined *a priori* using either a functional localizer obtained from published data (vmPFC; Figure 5A) or anatomical masks used in the literature (APC and PPC; Figure 5D). Using this approach, we found evidence for 6-fold modulation of the fMRI signal, with significant differences between aligned and misaligned trajectories, in vmPFC ($t_{27} = 2.94$, $p_{FDR} = 0.013$, one-sided; Figure 5B). However, the effect in vmPFC was not specific to a 6-fold symmetric profile, such that significant results were also observed for 3-fold symmetry ($t_{27} = 3.14$, $p = 0.002$, one-sided; Figure 5C). Of note, the 6-fold symmetric profile was not statistically different from the 3-fold symmetric model ($t_{27} = 1.632$, $p = 0.114$), leaving open the possibility that spatial periodicities other than those associated with a "true" grid code might otherwise explain the neural patterns in this region.

By comparison, activity in APC varied in a 6-fold symmetric manner ($t_{27} = 1.86$, $p_{FDR} = 0.049$, one-sided; Figure 5E), and this effect was specific to 6-fold symmetry (there was a trend toward significance for 5-fold symmetry: $t_{27} = 1.36$, $p = 0.093$, one-sided; all other control symmetries were not significant: $t_{27} < 0.96$, $p > 0.174$, one-sided; Figure 5F). These results indicate the presence of grid-like responses in APC. No significant effect was found in PPC ($t_{27} = 0.08$, $p_{FDR} = 0.468$, one-sided; Figure S4). Taken together, our findings are in line with previously published results[23] and suggest that only the anterior portion of piriform cortex, but not its posterior counterpart, is engaged during human olfactory navigation and may work together with ERC to support spatial performance when relying on the sense of smell.

Grid-like responses in ERC and APC are aligned to the same grid orientation

Evidence for grid-like responses in ERC and APC may indicate that these regions form a grid network that guides olfactory navigation. However, a true network would further require that the different brain regions be attuned to the same grid angle such that they can share orientation information in a common code. To test this possibility, we performed a cross-region consistency

Please cite this article in press as: Raithel et al., Recruitment of grid-like responses in human entorhinal and piriform cortices by odor landmark-based navigation, Current Biology (2023), https://doi.org/10.1016/j.cub.2023.06.087

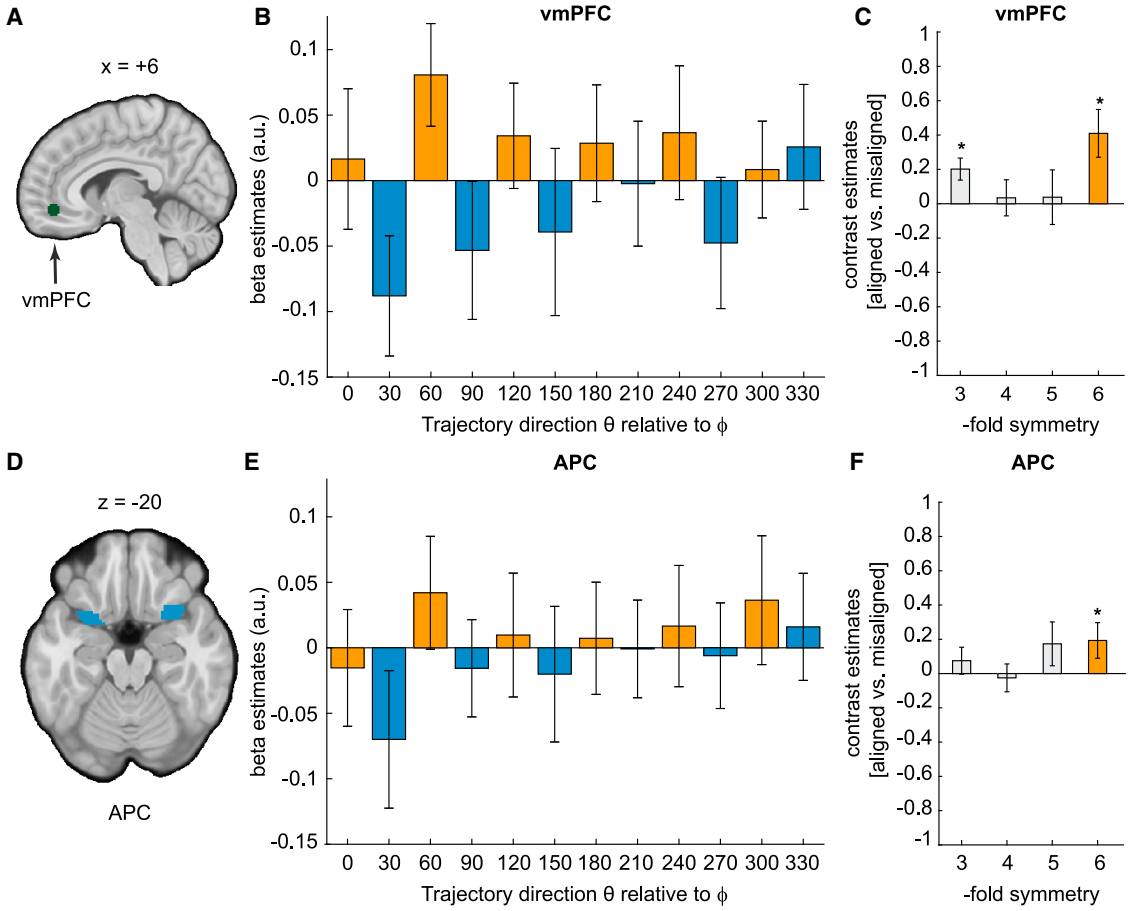

Figure 5. Grid-like responses in anterior piriform cortex (APC), but not ventromedial prefrontal cortex (vmPFC), during human olfactory navigation

(A) A functionally defined vmPFC mask (center MNI coordinates: x = 6, y = 46, z = −10, 5 mm sphere) was obtained from a prior study in our lab.[23]

(B) fMRI BOLD signal in vmPFC is higher in aligned compared with misaligned trials (t_{27} = 2.94, p_{FDR} = 0.013, one-sided).

(C) Sinusoidal modulation of the fMRI signal in vmPFC was found for not only 6-fold symmetry but also 3-fold symmetry (t = 3.14, p = 0.002, one-sided). None of the other control symmetries were significant (t < 0.33, p > 0.373, one-sided).

(D) Anatomical mask delineating APC.[23,43]

(E) Hexagonally modulated activity was detected in APC (aligned > misaligned; t_{27} = 1.86, p_{FDR} = 0.049, one-sided).

(F) There was a trend toward significance for 5-fold symmetry (t_{27} = 1.36, p = 0.093, one-sided); all other control symmetries were not significant (t_{27} < 0.96, p > 0.174, one-sided). See also Figures S3 and S4.

Data are mean ± SEM.

analysis in which we estimated the grid orientation from the rERC (using data from all but one run) to align movement trajectories in APC (in the left-out run) and then compared fMRI activity in APC during aligned vs. misaligned trajectories. Of note, the grid orientation in the rERC could be used to align activity in APC (t_{27} = 1.89, p = 0.035, one-sided; Figure 6A). Likewise, grid orientations in rERC and APC were positively correlated (r = 0.42, p = 0.042), and the difference in grid orientation between rERC and APC was not distributed uniformly but, instead, had a mean of 0° (V = 11.39, p = 0.001; Figure 6B). These results indicate that grid codes in APC and rERC share a common orientation, raising the idea that these regions form a functional network that emerges during human olfactory navigation. Finally, we tested whether the grid alignment between these two regions correlated with behavior, with the prediction being that greater alignment would yield better odor-based navigation performance. However, the corresponding test revealed no significant relationship between inter-regional grid alignment and the number of trials completed (r = −0.27, p = 0.165; Figure S6).

DISCUSSION

Humans are commonly described as visual navigators. However, it is rarely the case that behavior relies on a singular modality. Much more likely is that cues from multiple sensory domains can be used interchangeably, or in combination, to inform (spatial) behavior. In our study, we have shown that, contrary to common beliefs, humans can indeed use olfactory landmarks within a virtual environment to form a cognitive map and use this map to orient and navigate efficiently in space.

Our findings demonstrate that humans are able to apprehend olfactory cues as spatially stable landmarks, in line with rodent

Please cite this article in press as: Raithel et al., Recruitment of grid-like responses in human entorhinal and piriform cortices by odor landmark-based navigation, Current Biology (2023), https://doi.org/10.1016/j.cub.2023.06.087

CellPress
OPEN ACCESS

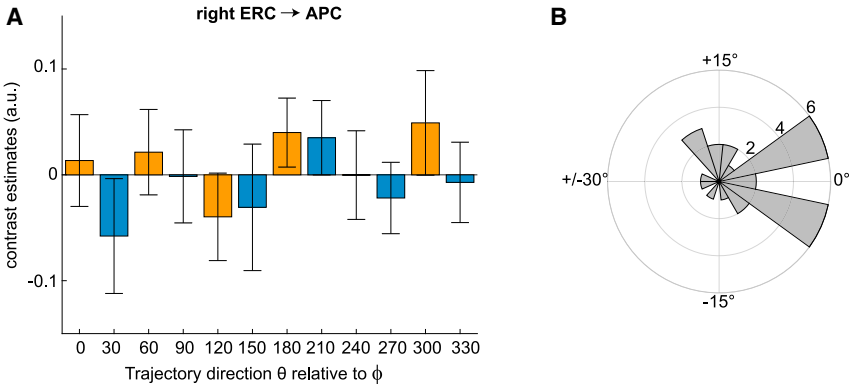

Figure 6. Grid-like responses in entorhinal and anterior piriform cortices were aligned to the same grid orientation

(A) Estimating grid orientation in right entorhinal cortex (rERC) and testing whether the resulting grid orientation yielded a significant effect of aligned vs. misaligned trajectories in anterior piriform cortex (APC) revealed that rERC and APC were aligned to the same grid orientation ($t_{27} = 1.89$, $p = 0.035$, one-sided). Data are mean ± SEM.

(B) Grid orientation in rERC and APC were positively correlated with one another ($r = 0.42$, $p = 0.042$), an effect that can be appreciated by looking at the distribution of angular differences between the estimated grid orientation in right ERC vs. APC across n = 28 participants. The angular difference between the estimated grid orientation in rERC vs. APC was not uniformly distributed around the circle but instead exhibited a mean of 0° ($V = 11.39$, $p = 0.001$). See also Figures S5 and S6.

literature,[26] and that they can use the relative relationships between odors to navigate in space. This conclusion is supported by the finding that our participants took more direct paths over the course of the experiment, allowing them to find the target odors more quickly and thus complete a greater number of trials. These results are fundamentally distinct from those described in prior studies due to substantial differences in experimental design: previous experiments either asked participants to associate specific spatial decisions (left vs. right turn) with specific odor identities[22] or involved the use of odor gradients.[23,24]

Although odor gradients may be the ecologically more relevant stimulus to probe olfactory navigation, our approach of using discrete olfactory stimuli allows us to draw direct comparisons to the existing and abundant literature on visually guided navigation. Such comparisons may provide useful insights, especially when evaluating the finding that olfactory navigation performance was lower at the beginning of each block. This finding was unexpected, leaving us to speculate whether participants thought of the odor clouds as intrinsically unstable, based on the more volatile nature of odors occurring in real-life environments. Although our instructions made it clear that the odor layout is constant across time, it could be that real-world experiences outside the laboratory biased participants to think that the layout would change. It would be interesting to see if such expectations, if present, could be "turned off" using visual landmarks.

More direct path-taking is one of the hallmarks of cognitive maps, inspiring confidence that our participants indeed used a corresponding map-like strategy. The use of cognitive maps is further supported by the finding of grid-like responses in ERC, an area traditionally associated with grid cells in rodents[33,34] as well as non-human[44] and human primates.[36] Our data are consistent with the existing literature reporting a grid-like code in ERC during virtual,[35] visual,[41,44,45] imagined,[46,47] and abstract[39] navigation; importantly, all of these studies used visual stimulus material to address their research questions. In contrast, our study used olfactory landmarks as the critical spatial cues, thereby suggesting that ERC, and particularly the rERC,[35,41] is crucial in mediating navigation behavior across multiple sensory domains.

Interestingly, our previous study[23] did not reveal grid-like responses in ERC using a univariate analysis approach. Rather, by taking advantage of a multivariate (multi-voxel) framework, we were able to identify a distributed hexa-directional coding scheme. One potential explanation for the discrepancy between these two studies, other than task differences per se, was the difference in fMRI acquisition parameters, which were optimized for signal recovery in ventral prefrontal and medial temporal regions, respectively. Specifically, in our 2019 study, we set the slice angle to 15° relative to the anterior-posterior commissure to minimize signal dropout in the basal frontal areas of the brain,[48,49] whereas in our present study, we did not adjust the slice angle to limit signal dropout in the medial temporal lobe.[50]

Another difference between the two studies concerns the evidence for grid-like coding in vmPFC. Although Bao and colleagues[23] reported grid-like coding in vmPFC, a similar effect in the current study was not specific to 6-fold rotational symmetry. Besides differences in fMRI acquisition protocols, this discrepancy could be due to differences in experimental design: in our prior study, we created a two-dimensional olfactory space using a set of binary (i.e., two-component) odor mixtures and asked participants to mentally "navigate" from one mixture to another by instructing them to adjust the intensity of the odor components.[23] This behavioral paradigm was markedly different from the veridical odor navigation task described here. Taken together, our findings prompt the question of whether odor navigation in abstract spaces[23] is distinct from odor navigation in physical or virtual spaces.

On the other hand, and in line with our previously published study,[23] we identified significant grid-like codes in APC, but not in PPC. Of note, grid-like codes in APC were aligned with the putative grid orientation in rERC, suggesting that APC and rERC may comprise a functional grid network during navigation critically relying on olfactory information. One possibility is that APC conveys information about the identity of odor landmarks to ERC in order to anchor the spatial map. Alternatively (or in addition), information about the location of target odors may be shared between the two regions to directly support the use of the cognitive map for odor-guided navigation. Of note, grid

alignment between rERC and APC was not correlated with navigation performance, presumably due to limited variability in behavioral performance as participants performed at ceiling at the time of scanning.

An open question is how the described grid network is established.[51] One possibility is that ERC is in fact the only region that contains grid cells, and grid-like responses in other regions, such as APC, are simply a byproduct of forward projections originating in ERC. In our previous study, we suggested that this mechanism may provide a plausible interpretation of grid-like responses outside of ERC.[23] Considering more recent evidence,[11,52,53] there seems to be at least one alternative possibility, namely, that regions other than ERC contain grid-cells[36] and that different populations of cells are brought into alignment through inter-areal connections during active navigation behavior. This interpretation is endorsed by findings from the rodent literature, showing that grid cells exist in visual[52] and somatosensory[53] cortices. Likewise, place cell-like neurons have been found in piriform cortex during an odor-cued spatial task.[11] It remains to be shown, however, whether "visual" and "somatosensory" grid cells, or likewise "olfactory" place cells, are active only during navigation guided by cues from the corresponding sensory modality or whether these neurons are active in generating multimodal sensory representations to optimize navigation behavior. To solve this question, it will also be relevant to consider the anatomical connections between regions within the grid network. For example, direct anatomical connections between piriform cortex and ERC are restricted to the lateral portion of ERC in both rodents,[27,28,30,31,54–56] and non-human primates,[16,57] whereas grid cells are typically reported in rodent medial ERC[33,34] and in non-human primate posterior-medial ERC.[44]

The finding that humans can navigate efficiently within a complex (virtual) olfactory landscape, critically relying on their noses to guide them, highlights the prowess of the human sense of smell, especially in the context of odor search and path finding. Our behavioral observations, broadly in line with a handful of other timely and relevant studies,[18–24] suggest that a paradigm shift in how to consider and value the human olfactory apparatus is well at hand. Taken together, with the demonstration of a grid-like network consisting of olfactory, limbic, and prelimbic brain areas, our findings offer new potential mechanisms and strategies for pushing the frontiers of understanding olfactory navigation. Finally, as suggested in our data, spatial information appears to be available at a very early stage of olfactory processing and may critically affect activity in other olfactory areas throughout the brain.

STAR★METHODS

Detailed methods are provided in the online version of this paper and include the following:

- KEY RESOURCES TABLE
- RESOURCE AVAILABILITY
  - Lead contact
  - Materials availability
  - Data and code availability
- EXPERIMENTAL MODEL AND SUBJECT DETAILS
- METHOD DETAILS
  - Odor stimuli and delivery
  - Odor ratings, odor naming task, and 4-AFC task
  - Odor navigation task
  - Respiratory recording and analysis
  - fMRI acquisition
  - Image pre-processing
  - General linear model (GLM) approach
  - Grid-orientation analysis
  - ROI definition
- QUANTIFICATION AND STATISTICAL ANALYSIS

SUPPLEMENTAL INFORMATION

Supplemental information can be found online at https://doi.org/10.1016/j.cub.2023.06.087.

ACKNOWLEDGMENTS

This work was supported by the National Institute on Deafness and Other Communication Disorders (NIDCD, grant R01DC019405 awarded to J.A.G.) and the Intramural Research Program at the National Institute on Drug Abuse (ZIA DA000642 awarded to T.K.). The opinions expressed in this work are the authors' own and do not reflect the view of the NIH/DHHS.

AUTHOR CONTRIBUTIONS

Conceptualization, data curation, formal analysis, investigation, methodology, software, visualization, writing – original draft, writing – review & editing, C.U.R.; software, A.J.M.; conceptualization, writing – review & editing, R.A.E.; conceptualization, supervision, writing – review & editing, T.K.; conceptualization, funding acquisition, resources, supervision, writing – review & editing, J.A.G.

DECLARATION OF INTERESTS

The authors declare no competing interests.

Received: February 24, 2023
Revised: May 23, 2023
Accepted: June 30, 2023
Published: July 27, 2023

REFERENCES

1. Baker, K.L., Dickinson, M., Findley, T.M., Gire, D.H., Louis, M., Suver, M.P., Verhagen, J.V., Nagel, K.I., and Smear, M.C. (2018). Algorithms for olfactory search across species. J. Neurosci. *38*, 9383–9389. https://doi.org/10.1523/JNEUROSCI.1668-18.2018.
2. Marin, A.C., Schaefer, A.T., and Ackels, T. (2021). Spatial information from the odour environment in mammalian olfaction. Cell Tissue Res. *383*, 473–483. https://doi.org/10.1007/s00441-020-03395-3.
3. Raithel, C.U., and Gottfried, J.A. (2021). Using your nose to find your way: ethological comparisons between human and non-human species. Neurosci. Biobehav. Rev. *128*, 766–779. https://doi.org/10.1016/j.neubiorev.2021.06.040.
4. Esquivelzeta Rabell, J., Mutlu, K., Noutel, J., Martin Del Olmo, P., and Haesler, S. (2017). Spontaneous rapid odor source localization behavior requires interhemispheric communication. Curr. Biol. CB *27*, 1542–1548.e4. https://doi.org/10.1016/j.cub.2017.04.027.
5. Findley, T.M., Wyrick, D.G., Cramer, J.L., Brown, M.A., Holcomb, B., Attey, R., Yeh, D., Monasevitch, E., Nouboussi, N., Cullen, I., et al. (2021). Sniff-synchronized, gradient-guided olfactory search by freely moving mice. eLife *10*, e58523, https://doi.org/10.7554/eLife.58523.

6. Gire, D.H., Kapoor, V., Arrighi-Allisan, A., Seminara, A., and Murthy, V.N. (2016). Mice develop efficient strategies for foraging and navigation using complex natural stimuli. Curr. Biol. *26*, 1261–1273. https://doi.org/10.1016/j.cub.2016.03.040.

7. Gumaste, A., Coronas-Samano, G., Hengenius, J., Axman, R., Connor, E.G., Baker, K.L., Ermentrout, B., Crimaldi, J.P., and Verhagen, J.V. (2020). A comparison between mouse, in silico, and robot odor plume navigation reveals advantages of mouse odor tracking. eNeuro *7*, ENEURO.0212-19.2019, https://doi.org/10.1523/ENEURO.0212-19.2019.

8. Kadakia, N., Demir, M., Michaelis, B.T., DeAngelis, B.D., Reidenbach, M.A., Clark, D.A., and Emonet, T. (2022). Odour motion sensing enhances navigation of complex plumes. Nature *611*, 754–761. https://doi.org/10.1038/s41586-022-05423-4.

9. Kikuta, S., Sato, K., Kashiwadani, H., Tsunoda, K., Yamasoba, T., and Mori, K. (2010). From the Cover: Neurons in the anterior olfactory nucleus pars externa detect right or left localization of odor sources. Proc. Natl. Acad. Sci. USA *107*, 12363–12368. https://doi.org/10.1073/pnas.1003999107.

10. Parabucki, A., Bizer, A., Morris, G., Munoz, A.E., Bala, A.D.S., Smear, M., and Shusterman, R. (2019). Odor concentration change coding in the olfactory bulb. eNeuro *6*, ENEURO.0396-18.2019, https://doi.org/10.1523/ENEURO.0396-18.2019.

11. Poo, C., Agarwal, G., Bonacchi, N., and Mainen, Z.F. (2022). Spatial maps in piriform cortex during olfactory navigation. Nature *601*, 595–599. https://doi.org/10.1038/s41586-021-04242-3.

12. Radvansky, B.A., and Dombeck, D.A. (2018). An olfactory virtual reality system for mice. Nat. Commun. *9*, 839, https://doi.org/10.1038/s41467-018-03262-4.

13. Zhang, S., and Manahan-Vaughan, D. (2015). Spatial olfactory learning contributes to place field formation in the hippocampus. Cereb. Cortex *25*, 423–432. https://doi.org/10.1093/cercor/bht239.

14. Dahmani, L., Patel, R.M., Yang, Y., Chakravarty, M.M., Fellows, L.K., and Bohbot, V.D. (2018). An intrinsic association between olfactory identification and spatial memory in humans. Nat. Commun. *9*, 4162, https://doi.org/10.1038/s41467-018-06569-4.

15. Dahmani, L., Courcot, B., Near, J., Patel, R., Amaral, R.S.C., Chakravarty, M.M., and Bohbot, V.D. (2020). Fimbria-fornix volume is associated with spatial memory and olfactory identification in humans. Front. Syst. Neurosci. *13*, 87.

16. Carmichael, S.T., Clugnet, M.-C., and Price, J.L. (1994). Central olfactory connections in the macaque monkey. J. Comp. Neurol. *346*, 403–434. https://doi.org/10.1002/cne.903460306.

17. Jacobs, L.F. (2012). From chemotaxis to the cognitive map: the function of olfaction. Proc. Natl. Acad. Sci. USA *109*, 10693–10700. https://doi.org/10.1073/pnas.1201880109.

18. Porter, J., Craven, B., Khan, R.M., Chang, S.J., Kang, I., Judkewitz, B., Volpe, J., Settles, G., and Sobel, N. (2007). Mechanisms of scent-tracking in humans. Nat. Neurosci. *10*, 27–29. https://doi.org/10.1038/nn1819.

19. Porter, J., Anand, T., Johnson, B., Khan, R.M., and Sobel, N. (2005). Brain mechanisms for extracting spatial information from smell. Neuron *47*, 581–592. https://doi.org/10.1016/j.neuron.2005.06.028.

20. Vonbekesy, G. (1964). Olfactory analogue to directional hearing. J. Appl. Physiol. *19*, 369–373. https://doi.org/10.1152/jappl.1964.19.3.369.

21. Wu, Y., Chen, K., Ye, Y., Zhang, T., and Zhou, W. (2020). Humans navigate with stereo olfaction. Proc. Natl. Acad. Sci. USA *117*, 16065–16071. https://doi.org/10.1073/pnas.2004642117.

22. Hamburger, K., and Knauff, M. (2019). Odors can serve as landmarks in human wayfinding. Cogn. Sci. *43*, e12798, https://doi.org/10.1111/cogs.12798.

23. Bao, X., Gjorgieva, E., Shanahan, L.K., Howard, J.D., Kahnt, T., and Gottfried, J.A. (2019). Grid-like neural representations support olfactory navigation of a two-dimensional odor space. Neuron *102*, 1066–1075.e5. https://doi.org/10.1016/j.neuron.2019.03.034.

24. Jacobs, L.F., Arter, J., Cook, A., and Sulloway, F.J. (2015). Olfactory orientation and navigation in humans. PLoS One *10*, e0129387, https://doi.org/10.1371/journal.pone.0129387.

25. Epstein, R.A., Patai, E.Z., Julian, J.B., and Spiers, H.J. (2017). The cognitive map in humans: spatial navigation and beyond. Nat. Neurosci. *20*, 1504–1513. https://doi.org/10.1038/nn.4656.

26. Fischler-Ruiz, W., Clark, D.G., Joshi, N.R., Devi-Chou, V., Kitch, L., Schnitzer, M., Abbott, L.F., and Axel, R. (2021). Olfactory landmarks and path integration converge to form a cognitive spatial map. Neuron *109*, 4036–4049.e5. https://doi.org/10.1016/j.neuron.2021.09.055.

27. Agster, K.L., and Burwell, R.D. (2009). Cortical efferents of the perirhinal, postrhinal, and entorhinal cortices of the rat. Hippocampus *19*, 1159–1186. https://doi.org/10.1002/hipo.20578.

28. Burwell, R.D., and Amaral, D.G. (1998). Cortical afferents of the perirhinal, postrhinal, and entorhinal cortices of the rat. J. Comp. Neurol. *398*, 179–205. https://doi.org/10.1002/(SICI)1096-9861(19980824)398:2<179::AID-CNE3>3.0.CO;2-Y.

29. Chen, Y., Chen, X., Baserdem, B., Zhan, H., Li, Y., Davis, M.B., Kebschull, J.M., Zador, A.M., Koulakov, A.A., and Albeanu, D.F. (2022). High-throughput sequencing of single neuron projections reveals spatial organization in the olfactory cortex. Cell *185*, 4117–4134.e28. https://doi.org/10.1016/j.cell.2022.09.038.

30. Leitner, F.C., Melzer, S., Lütcke, H., Pinna, R., Seeburg, P.H., Helmchen, F., and Monyer, H. (2016). Spatially segregated feedforward and feedback neurons support differential odor processing in the lateral entorhinal cortex. Nat. Neurosci. *19*, 935–944. https://doi.org/10.1038/nn.4303.

31. Kerr, K.M., Agster, K.L., Furtak, S.C., and Burwell, R.D. (2007). Functional neuroanatomy of the parahippocampal region: the lateral and medial entorhinal areas. Hippocampus *17*, 697–708. https://doi.org/10.1002/hipo.20315.

32. Bush, D., Barry, C., and Burgess, N. (2014). What do grid cells contribute to place cell firing? Trends Neurosci. *37*, 136–145. https://doi.org/10.1016/j.tins.2013.12.003.

33. Hafting, T., Fyhn, M., Molden, S., Moser, M.-B., and Moser, E.I. (2005). Microstructure of a spatial map in the entorhinal cortex. Nature *436*, 801–806. https://doi.org/10.1038/nature03721.

34. Stensola, H., Stensola, T., Solstad, T., Frøland, K., Moser, M.B., and Moser, E.I. (2012). The entorhinal grid map is discretized. Nature *492*, 72–78. https://doi.org/10.1038/nature11649.

35. Doeller, C.F., Barry, C., and Burgess, N. (2010). Evidence for grid cells in a human memory network. Nature *463*, 657–661. https://doi.org/10.1038/nature08704.

36. Jacobs, J., Weidemann, C.T., Miller, J.F., Solway, A., Burke, J.F., Wei, X.-X., Suthana, N., Sperling, M.R., Sharan, A.D., Fried, I., et al. (2013). Direct recordings of grid-like neuronal activity in human spatial navigation. Nat. Neurosci. *16*, 1188–1190. https://doi.org/10.1038/nn.3466.

37. Barry, C., Hayman, R., Burgess, N., and Jeffery, K.J. (2007). Experience-dependent rescaling of entorhinal grids. Nat. Neurosci. *10*, 682–684. https://doi.org/10.1038/nn1905.

38. Keinath, A.T. (2016). The preferred directions of conjunctive grid X Head direction cells in the medial entorhinal cortex are periodically organized. PLoS One *11*, e0152041, https://doi.org/10.1371/journal.pone.0152041.

39. Constantinescu, A.O., O'Reilly, J.X., and Behrens, T.E.J. (2016). Organizing conceptual knowledge in humans with a gridlike code. Science *352*, 1464–1468. https://doi.org/10.1126/science.aaf0941.

40. Maass, A., Berron, D., Libby, L.A., Ranganath, C., and Düzel, E. (2015). Functional subregions of the human entorhinal cortex. eLife *4*, e06426, https://doi.org/10.7554/eLife.06426.

41. Nau, M., Navarro Schröder, T., Bellmund, J.L.S., and Doeller, C.F. (2018). Hexadirectional coding of visual space in human entorhinal cortex. Nat. Neurosci. *21*, 188–190. https://doi.org/10.1038/s41593-017-0050-8.

42. Park, S.A., Miller, D.S., and Boorman, E.D. (2021). Inferences on a multidimensional social hierarchy use a grid-like code. Nat. Neurosci. *24*, 1292–1301. https://doi.org/10.1038/s41593-021-00916-3.

43. Mai, J.K., Majtanik, M., and Paxinos, G. (2015). Atlas of the Human Brain (Academic Press).

44. Killian, N.J., Jutras, M.J., and Buffalo, E.A. (2012). A map of visual space in the primate entorhinal cortex. Nature *491*, 761–764. https://doi.org/10.1038/nature11587.

45. Julian, J.B., Keinath, A.T., Frazzetta, G., and Epstein, R.A. (2018). Human entorhinal cortex represents visual space using a boundary-anchored grid. Nat. Neurosci. *21*, 191–194. https://doi.org/10.1038/s41593-017-0049-1.

46. Bellmund, J.L., Deuker, L., Navarro Schröder, T., and Doeller, C.F. (2016). Grid-cell representations in mental simulation. eLife *5*, e17089, https://doi.org/10.7554/eLife.17089.

47. Horner, A.J., Bisby, J.A., Zotow, E., Bush, D., and Burgess, N. (2016). Grid-like processing of imagined navigation. Curr. Biol. *26*, 842–847. https://doi.org/10.1016/j.cub.2016.01.042.

48. Deichmann, R., Gottfried, J.A., Hutton, C., and Turner, R. (2003). Optimized EPI for fMRI studies of the orbitofrontal cortex. NeuroImage *19*, 430–441. https://doi.org/10.1016/S1053-8119(03)00073-9.

49. Weiskopf, N., Hutton, C., Josephs, O., and Deichmann, R. (2006). Optimal EPI parameters for reduction of susceptibility-induced BOLD sensitivity losses: A whole-brain analysis at 3 T and 1.5 T. NeuroImage *33*, 493–504. https://doi.org/10.1016/j.neuroimage.2006.07.029.

50. Nau, M. (2019). Functional imaging of the human medial temporal lobe. https://doi.org/10.17605/OSF.IO/CQN4Z.

51. Raithel, C.U., and Gottfried, J.A. (2021). What are grid-like responses doing in the orbitofrontal cortex? Behav. Neurosci. *135*, 218–225. https://doi.org/10.1037/bne0000453.

52. Long, X., Deng, B., Cai, J., Chen, Z.S., and Zhang, S.-J. (2021). A compact spatial map in V2 visual cortex. https://doi.org/10.1101/2021.02.11.430687.

53. Long, X., and Zhang, S.-J. (2021). A novel somatosensory spatial navigation system outside the hippocampal formation. Cell Res. *31*, 649–663. https://doi.org/10.1038/s41422-020-00448-8.

54. Chapuis, J., Cohen, Y., He, X., Zhang, Z., Jin, S., Xu, F., and Wilson, D.A. (2013). Lateral entorhinal modulation of piriform cortical activity and fine odor discrimination. J. Neurosci. *33*, 13449–13459. https://doi.org/10.1523/JNEUROSCI.1387-13.2013.

55. Luskin, M.B., and Price, J.L. (1983). The laminar distribution of intracortical fibers originating in the olfactory cortex of the rat. J. Comp. Neurol. *216*, 292–302. https://doi.org/10.1002/cne.902160306.

56. Price, J.L. (1973). An autoradiographic study of complementary laminar patterns of termination of afferent fibers to the olfactory cortex. J. Comp. Neurol. *150*, 87–108. https://doi.org/10.1002/cne.901500105.

57. Insausti, R., Marcos, P., Arroyo-Jiménez, M.M., Blaizot, X., and Martínez-Marcos, A. (2002). Comparative aspects of the olfactory portion of the entorhinal cortex and its projection to the hippocampus in rodents, nonhuman primates, and the human brain. Brain Res. Bull. *57*, 557–560. https://doi.org/10.1016/S0361-9230(01)00684-0.

58. Gorgolewski, K.J., Varoquaux, G., Rivera, G., Schwarz, Y., Ghosh, S.S., Maumet, C., Sochat, V.V., Nichols, T.E., Poldrack, R.A., Poline, J.-B., et al. (2015). NeuroVault.org: a web-based repository for collecting and sharing unthresholded statistical maps of the human brain. Front. Neuroinform. *9*, 8.

59. Brainard, D.H. (1997). The psychophysics toolbox. Spat. Vis. *10*, 433–436. https://doi.org/10.1163/156856897X00357.

60. Berens, P. (2009). CircStat: a MATLAB toolbox for circular statistics. J. Stat. Softw. *31*, 1–21. https://doi.org/10.18637/jss.v031.i10.

61. Eickhoff, S.B., Stephan, K.E., Mohlberg, H., Grefkes, C., Fink, G.R., Amunts, K., and Zilles, K. (2005). A new SPM toolbox for combining probabilistic cytoarchitectonic maps and functional imaging data. NeuroImage *25*, 1325–1335. https://doi.org/10.1016/j.neuroimage.2004.12.034.

62. Maldjian, J.A., Laurienti, P.J., Kraft, R.A., and Burdette, J.H. (2003). An automated method for neuroanatomic and cytoarchitectonic atlas-based interrogation of fMRI data sets. NeuroImage *19*, 1233–1239. https://doi.org/10.1016/S1053-8119(03)00169-1.

63. Green, B.G., Dalton, P., Cowart, B., Shaffer, G., Rankin, K., and Higgins, J. (1996). Evaluating the 'labeled magnitude scale' for measuring sensations of taste and smell. Chem. Senses *21*, 323–334. https://doi.org/10.1093/chemse/21.3.323.

64. Lim, J., Wood, A., and Green, B.G. (2009). Derivation and evaluation of a labeled hedonic scale. Chem. Senses *34*, 739–751. https://doi.org/10.1093/chemse/bjp054.

65. Howard, J.D., and Kahnt, T. (2018). Identity prediction errors in the human midbrain update reward-identity expectations in the orbitofrontal cortex. Nat. Commun. *9*, 1611, https://doi.org/10.1038/s41467-018-04055-5.

Please cite this article in press as: Raithel et al., Recruitment of grid-like responses in human entorhinal and piriform cortices by odor landmark-based navigation, Current Biology (2023), https://doi.org/10.1016/j.cub.2023.06.087

STAR★METHODS

KEY RESOURCES TABLE

REAGENT or RESOURCE	SOURCE	IDENTIFIER
Deposited data		
Whole Brain t-maps	Neurovault[58]: https://neurovault.org/collections/TPTJBHBU/	RRID: SCR_003806
Source Data	Open Science Framework (OSF): https://doi.org/10.17605/OSF.IO/SN9XV	RRID: SCR_003238
Software and algorithms		
Unity3D 2018.4.23f1	Unity Technologies, https://unity.com/	N/A
MATLAB 2019a, 2021a	MathWorks, https://www.mathworks.com/products/matlab.html	RRID: SCR_001622
Psychophysics Toolbox, Version 3	Brainard[59], http://psychtoolbox.org/	RRID: SCR_002881
SPM12	The Wellcome Trust Centre for Neuroimaging, https://www.fil.ion.ucl.ac.uk/spm/software/spm12/	RRID: SCR_007037
CircStat	Berens[60], http://bethgelab.org/software/circstat/	RRID: SCR_016651
Anatomy Toolbox	Eickhoff et al.[61], https://www.fz-juelich.de/de/inm/inm-1/downloads/toolbox/toolbox_22	RRID: SCR_013273
WFU Pickatlas	Maldjian et al.[62], https://www.nitrc.org/projects/wfu_pickatlas/	RRID: SCR_007378

RESOURCE AVAILABILITY

Lead contact

Further information and requests for resources and reagents should be directed to and will be fulfilled by the lead contact, Clara U. Raithel (raithelc@sas.upenn.edu).

Materials availability

This study did not generate new unique reagents.

Data and code availability

The source data to reproduce all figures have been deposited at Open Science Framework and are publicly available at the time of publication. In addition, t-maps showing the whole-brain results for cross-regional cross-validation analyses were made available on Neurovault. Respective links are listed in the key resources table. This paper does not report original code. Any additional information required to reanalyze the data reported in this paper is available from the lead contact upon request.

EXPERIMENTAL MODEL AND SUBJECT DETAILS

Twenty-eight participants (13 women; aged 18-38 years, mean = 25.69, SD = 4.88) completed this study. Thirty-three participants (16 women, aged 18-38 years, mean = 25.97, SD = 4.83) gave informed consent as approved by the University of Pennsylvania Institutional Review Board (protocol #833173). During screening, all participants indicated to have an average (or better than average) sense of smell and reported to be right-handed non-smokers with no history of significant medical illness, psychiatric disorder or olfactory dysfunction. Following the invitation to the laboratory, participants performed two training sessions (day 1 and day 2) which comprised odor ratings, an odor naming task, a four-alternative forced choice (4-AFC) task, and an odor navigation task. Twenty-eight participants who completed at least 35 trials of the odor navigation task on day 2 (i.e., ~50% of the average number of trials completed across subjects) took part in two fMRI scanning sessions with the same odor navigation task on day 3 and day 4 (Figure 1). All participants were given monetary compensation for their time.

METHOD DETAILS

Odor stimuli and delivery

Stimuli for the experiment included eight familiar odors: eucalyptus, orange, vanilla, rose, baby powder, banana, peanut butter and almond. The first four odors were obtained from essential oils (NOW Essential Oils, Boomingdale, IL, USA; Aura Cacia, Norway, IA)

Please cite this article in press as: Raithel et al., Recruitment of grid-like responses in human entorhinal and piriform cortices by odor landmark-based navigation, Current Biology (2023), https://doi.org/10.1016/j.cub.2023.06.087

which were diluted in mineral oil (Sigma Aldrich, St. Louis, MO, USA) at different concentrations to yield similar levels of perceived intensity (eucalyptus: 5%; orange: 15%; vanilla: 25%; rose: 25%). Baby powder, banana and peanut butter were retrieved from natural products that can be purchased in standard local supermarkets. Specifically, we used 5.1g of Johnson's Baby Powder lotion, 6.1g of a freshly cut banana, and 5.0g of peanut butter. Finally, benzaldehyde (Sigma Aldrich, St. Louis, MO, USA) was diluted in mineral oil (Sigma Aldrich, St. Louis, MO, USA) to obtain almond odor (0.5%). All odors were stored in amber bottles and delivered to the participant using a custom-built, computer-controlled 12-channel olfactometer. In this system, clean or odorized air was directed toward the participant (wearing a nasal mask) via Teflon tubing at a constant rate of 3.2L/min. The control of air valves was achieved using customized scripts implemented in and Unity3D (Version 2018.4.23f1, Unity Technologies, https://unity.com/) and MATLAB (Version 2019a, The Mathworks Inc., Natick, MA, USA, https://www.mathworks.com/products/matlab.html).

Odor ratings, odor naming task, and 4-AFC task

On day 1, participants rated the intensity (on the General Labeled Magnitude Scale (gLMS),[63] pleasantness (on the Labeled Hedonic Scale (LHS)[64] and familiarity (on a visual analogue scale (VAS), bounded by 'not familiar at all' at the bottom and 'very familiar' at the top, corresponding to a value of 0 and 100, respectively) of each odor (one trial per odor). In addition to these perceptual ratings, participants were asked to name the odor that they had just smelled ('odor naming task', see Figure 1C). After the experimenter had ensured that participants had the correct label for each odor available, a four-alternative forced choice (4-AFC) task was performed. For this task, participants were again presented with each odor once, and asked to pick the correct label out of four answer options. All perceptual ratings, odor naming and odor discrimination were collected and recorded using Psychophysics Toolbox Version 3 (http://psychtoolbox.org/)[59] running on MATLAB.

Odor navigation task

During the training sessions (day 1 and day 2) and the fMRI scanning sessions (day 3 and day 4), participants performed an odor navigation task. The task comprised a virtual arena in which the eight odors introduced above were associated with distinct locations in space. The goal of the task was to find the odors as quickly as possible.

The virtual environment was created using Unity3D (Version 2018.4.23f1, Unity Technologies, https://unity.com/), and consisted of a circular arena with a radius of 50 virtual meters (vm). The unique location of the eight odors was marked by identical white clouds hovering over different locations of the grassy terrain. One odor cloud was located in the center of the arena, while the remaining seven clouds were arranged in the periphery of the circular environment, at 40 vm distance from the center (Figure 1A). This spatial layout was critical, as the visual cues present in the arena (the wall, the white clouds, the sky and the ground) did not give away any directional information: the only way participants could orient within the arena is to use olfactory cues.

At the beginning of a block, participants were placed inside one of the eight clouds, facing either toward the center of the arena (when dropped in the periphery), or outward at random (when dropped in the center of the arena). At this point, the white cloud changed its color to blue, cueing the participant to smell the odor associated with the participants' current location. At the same time, participants were presented with an instruction indicating which odor to search for (e.g., "Find the vanilla smell!"). After 3 seconds, the cloud turned white again and stopped emitting its odor; likewise, the instruction disappeared. Participants were then able to move freely and explore the environment in search for the target odor (Figure 1B).

When navigating through the virtual space, participants moved forward at a constant speed of five virtual meters per second by pressing the middle button of a response button box. In search of the odors, participants adjusted their heading direction by pressing the left or right button. Note that participants could move forward and change their walking direction simultaneously; however, they could not move backward.

Once participants had successfully located the target odor, they would receive feedback ("Well Done!") and, after a short inter-trial interval (ITI; on average: 4 seconds, range: 2-6 seconds), an instruction to find the next (target) odor. The selection of target odors was pseudorandomized such that all eight odors served as the target exactly once across eight trials. This allowed us to control the participants' exposure to the different odors and ensure relatively equal sampling of movement trajectories across space (Figures 1E and S1).

Participants completed eight blocks of the odor navigation task, so that on each block, participants started in one of the eight odor clouds as defined above. Each block was 4 minutes long, resulting in a total duration of 32 minutes per session.

Importantly, the spatial arrangement of odor clouds, although randomized across participants, was fixed across the entire experiment (from day 1 through day 4) for a given participant to optimize learning. At the beginning of the experiment, participants had to explore and learn the spatial arrangement of odors in the arena using a trial-and-error strategy. Once the spatial layout of odor landmarks was learned, participants were able to make a direct trajectory to the target odor. The only exception to this rule occurred in blocks in which the participants started in the center cloud, facing outward at random. In this particular instance, participants could not know where the other odors are relative to themselves, even after having learned the relative positions of the odors to one another. Because of this unique situation, these trials were excluded from all subsequent analyses (note that this affected only one individual trial per session, i.e., four trials per participant, and this number was consistent across participants).

Respiratory recording and analysis

During all experimental sessions, breathing activity was monitored using an MRI-compatible respiratory effort band (BIOPAC Systems Inc., Goleta, CA) fixed around the subjects' torso and recorded using PowerLab equipment (ADInstruments, Dunedin, New

Please cite this article in press as: Raithel et al., Recruitment of grid-like responses in human entorhinal and piriform cortices by odor landmark-based navigation, Current Biology (2023), https://doi.org/10.1016/j.cub.2023.06.087

Zealand) at a sampling frequency of 1kHz. Breathing traces from each individual block were smoothed using a moving window of 250ms, high-pass filtered (cutoff, 20s) to remove low-frequency drifts, and scaled to have a mean of 0 and a standard deviation of 1.[65] The cued sniff waveforms were extracted from the resulting breathing traces on a trial-by-trial basis. Subsequently, inhalation duration and volume were computed and used as nuisance regressors in statistical modeling of the fMRI data (see below). In a final step, breathing traces from each block were down-sampled to 0.5Hz to match the temporal resolution of the fMRI acquisition (2 seconds) and also included as nuisance regressors in statistical modeling of the fMRI data (see below). Data from five behavioral testing sessions (three on respective subjects' day 1, two on day 2) were missing due to technical problems. The respective panels in Figure S2 thus are based on n=25 and n=26, respectively.

fMRI acquisition

Imaging was performed on a 3 Tesla MRI scanner (PRISMA, Siemens Medical Systems) located at the University of Pennsylvania. Participants were placed comfortably in the scanner with their heads fixated using foam pads. Mounted on the 64-channel head coil was a mirror through which participants could see the virtual arena projected on a screen placed outside the scanner. The nasal mask as well as the Teflon tubing through which odorized air would be directed to the participant's nose were attached to the participant while they were lying on the examination bed. Gradient echo T2*-weighted echo-planar images (EPIs) were acquired using the following settings: repetition time (TR) = 2000ms, echo time (TE) = 22ms, flip angle = 80°, matrix size = 104 x 104, field of view (FoV) = 208mm, voxel size = 2x2x2mm^3, 58 slices per volume, multiband factor = 2. A single whole brain EPI (settings: repetition time (TR) = 2000ms, echo time (TE) = 22ms, flip angle = 60°, matrix size = 104 x 104, field of view (FoV) = 208mm, voxel size = 2x2x2mm^3, 81 slices per volume, multiband factor = 3) and a 0.9x0.9x1mm^3 T1-weighted structural MRI scan were also obtained to facilitate normalization of functional images into standard space.

Image pre-processing

fMRI data were pre-processed using SPM12 software (SPM software package, Wellcome Department, London, UK, https://fil.ion.ucl.ac.uk/spm) run in MATLAB (Version 2021a, The Mathworks Inc., Natick, MA, USA, https://www.mathworks.com/products/matlab.html). Preprocessing included 3D motion correction to compensate for small head movements by spatially aligning all functional images the first image in the time series. The two T1-weighted structural images and the two whole-brain EPI images were also spatially realigned, and resulting mean images were used for co-registering the functional images to the T1-weighted structural image. For spatial normalization of images to a standardized template, the structural image was normalized to the Montreal Neurological Institute (MNI) space using the six tissue probability maps provided by SPM12. The deformation fields were subsequently applied to functional images. Finally, spatial smoothing was applied to the data using a Gaussian kernel of 6mm FWHM.

General linear model (GLM) approach

Following image pre-processing, the fMRI time series was modeled using two general linear models (GLMs), one to estimate the grid orientation in a set of anatomical ROIs, and one to subsequently predict the fMRI BOLD signal based on the estimated grid orientation. Both GLMs shared a number of regressors, including eight odor events (one for each odor identity, or odor cloud), convolved with the canonical hemodynamic response function (HRF) in SPM12, as well as several nuisance regressors to account for head motion and breathing. More specifically, nuisance regressors included the following: the six movement parameters derived from spatial realignment, within-volume slice variance and odd-versus-even slice differences to account for within-scan motion, their derivatives and squares, the down-sampled breathing trace, as well as trial-by-trial sniff volume and sniff duration, both convolved with the HRF and orthogonalized with the sniff events. Additional nuisance regressors were introduced where needed to exclude individual volumes with excessive head motion. We defined volumes with ''excessive head motion'' as images for which (at least) one of the motion-correction parameters deviated 6SD of the mean. On average, 16 volumes (<1%; range 0-51) were excluded from each participant, out of a total of 2080 fMRI images (130 per run, 8 runs per session, 2 sessions per participant) acquired for the purpose of the present study. In both GLMs, data were high-pass filtered at 1/128 Hz and temporal autocorrelation was adjusted using an AR(1) process.

Grid-orientation analysis

A leave-one-out cross-validation analysis was performed to estimate the orientation of the grid code during periods of movement, following procedures used previously to identify grid-like codes during virtual navigation.[23,39] Each subject completed 16 fMRI scanning runs (8 runs * 2 sessions). Hence, for each participant, we estimated the grid orientation using each possible set of 15 fMRI scanning runs (training data), and then used the resulting grid orientation to predict a grid signal in the remaining, independent fMRI scanning run (testing data).

To estimate the grid orientation in the training data, we specified a GLM (GLM1) in which the movement period between two consecutively visited odor clouds was defined as the event of interest. For this regressor, we specified two parametric modulators, $\cos(6\theta)$ and $\sin(6\theta)$, where θ is the participant's average movement direction when navigating toward the next cloud. The beta weights of these parametric modulators (β_{cos} and β_{sin}) were fitted to the fMRI series for each voxel. The grid orientation within a-priori defined ROIs was then calculated as the mean beta weights across all voxels of a given ROI as $\varphi = [\arctan(\beta_{sin} / \beta_{cos})] / 6$ (note that the arctan was mapped into the 360° space before being divided by 6).

Please cite this article in press as: Raithel et al., Recruitment of grid-like responses in human entorhinal and piriform cortices by odor landmark-based navigation, Current Biology (2023), https://doi.org/10.1016/j.cub.2023.06.087

To test whether the grid orientation determined in the training data replicated in the testing data, we aligned the movement trajectories of the left-out-run relative to the presumed grid orientation φ in each participant, and divided the movement trajectories into 12 bins (0°±15, 30°±15, 60°±15, 90°±15, 120°±15, 150°±15, 180°±15, 210°±15, 240°±15, 270°±15, 300°±15, 330°±15) evenly spread around the unit circle (Figure 3). For each bin, a separate regressor was specified and estimated using the fMRI time series (GLM2). At the group level, we extracted the resulting 12 beta weights from the anatomical ROIs, and tested whether the beta estimates for aligned trajectories were higher than the beta estimates for misaligned trials (Figure 3). We also conducted control analyses with 3-, 4-, and 5-fold periodicity. For these analyses, the same approach was used, but φ was estimated with factor 3 (or 4, or 5), and all conditions were separated into 6 (or 8, or 10) bins of various degrees (60, 45, or 36°). Of note, the above procedure was also used to test for consistency of the grid orientation across different ROIs (by estimating the grid orientation in one ROI, and testing it in another). T-maps showing the whole-brain results for cross-regional cross-validation analyses were made available on neurovault.org[58] (https://neurovault.org/collections/TPTJBHBU/). In addition to the maps provided online, we also added whole-brain maps at two arbitrarily chosen thresholds ($p<0.001$ and $p<0.01$, uncorrected) to the supplementary information (Figure S3).

A brain region's activity was considered in line with a putative grid-cell population response, or 'grid-like', if the following conditions were met:

1) Significant hexa-directional (6-fold) modulation of the fMRI BOLD signal within this region
2) No significant effect for control symmetries (3-, 4-, and 5-fold),
   OR
   If there was a significant effect for one of the control symmetries, then the model using 6-fold modulation should provide a better fit than the respective control models.

ROI definition

Entorhinal cortex (ERC) was defined anatomically using a mask in MNI space made available online via an existing study.[40] Anatomically defined masks for anterior piriform cortex (APC) and posterior piriform cortex (PPC) were obtained from Bao and colleagues.[23,43] Ventromedial prefrontal cortex (vmPFC) was functionally defined using an independent dataset[23]; more specifically, vmPFC was defined as a 5mm sphere centered on the reported peak coordinates for hexa-directionally modulated activity (center MNI coordinates: x=6,y=46,z=-10).

In addition to our a-priori defined regions of interest, a number of additional (control) regions were included (Figure S4): early visual cortex (EVC) and posterior parietal cortex (both anatomically defined using the Anatomy Toolbox[61] in SPM12), as well as dorsolateral prefrontal cortex (dlPFC; anatomically defined using the WFU Pickatlas[62] in SPM12).

QUANTIFICATION AND STATISTICAL ANALYSIS

Error bars used in figures throughout the paper depict the mean ± standard error of the mean (SEM) across subjects ($n = 28$). In figures showing the contrast of aligned versus misaligned conditions with 60° periodicity, data were mean-corrected within subjects. The significance threshold was set at $p < 0.05$ one-tailed for testing brain areas showing effects of aligned > misaligned directions, based on our directional hypotheses.[45] Significance threshold was otherwise set to $p < 0.05$ two-tailed. Whenever multiple ROIs were tested, p-values were corrected for multiple testing across ROIs using the false discovery rate (FDR) correction (Benjamini-Hochberg method as implemented in MATLAB's *mafdr* function). Grid angle distributions were tested for using the Rayleigh test of circular non-uniformity using CircStat within MATLAB.[60] When testing the correlation of grid angle between ROIs, a circular correlation was computed using CircStat's *circ_corrcc* function. To test whether the angular difference in mean grid orientation between ROIs is distributed around a mean of zero CircStat's *circ_vtest* function was used.